

FIG. 1. The shift in the  $F^{19}$  resonance field from  $\omega/\gamma_F$  vs the external magnetic field. The dotted curve represents the predicted paramagnetic shift when  $H_0$  is parallel to the  $b$  axis and is given by Eq. (1).

At  $310^\circ\text{K}$ , with  $H_0 \perp b$ , a line was observed which differed from  $\omega/\gamma_F$  by an amount we designate by  $\Delta H$ ;  $\Delta H$  is plotted vs  $H_0$  in Fig. 1. It is to be noticed that  $\Delta H$  is proportional to  $H_0$  and is  $\sim 30$  times larger than the "paramagnetic shift" expected. The "paramagnetic shift" arises from the time averaged magnetic field at the  $F^{19}$  position due to the paramagnetic  $Mn^{++}$  ions. Its magnitude for temperatures greater than the transition temperature can be shown to be

$$\Delta H \simeq \frac{g^2 \beta^2 H_0 S(S+1)}{3k(T+\Theta)} \sum_i \frac{(1-3\cos^2\theta_{ij})}{r_{ij}^3}, \quad (1)$$

where the summation is over the  $Mn^{++}$  sites,  $\theta_{ij}$  is the angle between  $r_{ij}$  and  $H_0$  and the other symbols are conventional. In addition,  $\Delta H$  depended upon the temperature. The experimental values are, for 15.33 Mc/sec:  $T=310^\circ\text{K}$ ,  $\Delta H=118$  oe;  $T=195^\circ\text{K}$ ,  $\Delta H=150$  oe;  $T=77^\circ\text{K}$ ,  $\Delta H=257$  oe. These values roughly agree with the temperature dependence of Eq. (1).

In Fig. 2 the measured separation of the two resolved lines is plotted as a function of the angle between  $H_0$  and the  $b$  axis at 15.33 Mc/sec and  $77^\circ\text{K}$ . There is

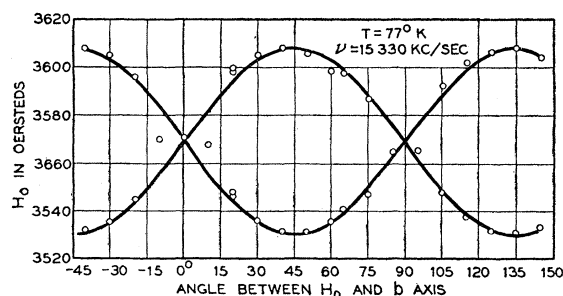


FIG. 2. Resonant magnetic field for  $F^{19}$  nuclei vs angle between  $H_0$  and the  $b$  axis with  $H_0$  in the  $a$ - $b$  plane. The theoretical angular dependence including contributions from near neighbors only is indicated, normalized to the amplitudes of the experimental data at  $\Phi=45^\circ$ .

plotted as well (solid line) the theoretical angular dependence, where we have only included contributions from the three nearest  $Mn^{++}$  normalized to a best fit with the experimental points. From the paramagnetic shift at this field and temperature, one calculates an extreme splitting of 60 oe and an average displacement of 7 oe from  $\omega/\gamma_F$ . These values are to be compared with the observed extreme splitting of 77 oe and the observed mean shift of 277 oe, when we include the demagnetizing correction for our spherical sample.

When the lines were resolved it was possible to determine that they were Lorentzian in shape. In addition, the signal-to-noise ratio was directly proportional to  $H_1$  indicating that  $(\gamma H_1)^2 T_1 T_2 \ll 1$ . This suggests that the observed line widths of the resolved lines (28.5 oe peak to peak of the derivative curve) arise from uncertainty broadening and that  $T_1 = T_2 = 1.6 \times 10^{-6}$  sec at  $77^\circ\text{K}$ . The unresolved line widths at  $310^\circ\text{K}$  are consistent with this value. Considering the line widths to be determined by the observed hyperfine interaction and exchange narrowing, one can calculate  $T_1 \sim 2 \times 10^{-6}$  sec.

At  $68^\circ\text{K}$ , corresponding to the antiferromagnetic transition temperature, the lines disappear.

The most reasonable explanation of the large shift is to suppose that an electron of the closed fluorine shell is promoted to the  $Mn^{++}$  ion and that the  $F^{19}$  nucleus is immersed in the large magnetic field of its own unpaired electrons for some part of the time. The magnitude of this field may be estimated from the calculated  $\psi^2(0)$  for an  $s$  electron. The fraction of the time that the electron is unpaired can then be calculated to be 2.5%. This promotion of the fluorine electron is the superexchange<sup>2</sup> mechanism and we see that nuclear magnetic resonance can provide a direct measure of superexchange.

We should like to thank P. W. Anderson for stimulating discussions about the applicability of superexchange, B. J. Wyluda for experimental assistance, E. F. Dearborn for growing the crystals, and J. F. Dillon, Jr., for helping to prepare samples.

<sup>1</sup> N. Bloembergen and N. J. Pouls, *Physica* **16**, 915 (1950); N. Bloembergen, *Physica* **16**, 95 (1950).

<sup>2</sup> P. W. Anderson, *Phys. Rev.* **79**, 350 (1950).

## Nuclear Magnetic Resonance of $Si^{29}$ in $n$ - and $p$ -Type Silicon

R. G. SHULMAN AND B. J. WYLUDA

*Bell Telephone Laboratories, Murray Hill, New Jersey*

(Received June 29, 1956)

WE have observed the nuclear magnetic resonances of  $Si^{29}$  in high purity silicon at room temperature and have determined the spin-lattice relaxation time as a function of sample resistivity. The resonance lines were observed with a Varian Associates variable-

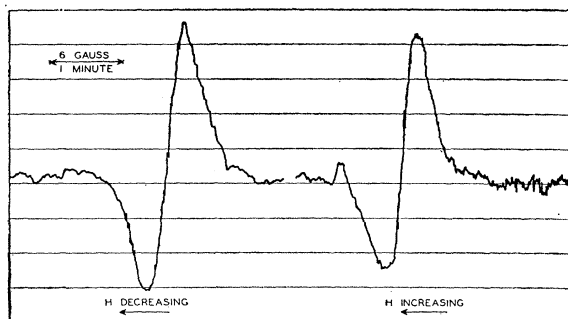


FIG. 1. Recorder plot of adiabatic fast-passage dispersion derivative. In this plot  $H_1 \sim 3$  gauss  $\gg 1/\gamma T_2 \gg 1/\gamma T_1$ . Modulation is 100 cps and  $\sim 2$  gauss. Notice that the phase of line changes by  $\pi$  as a result of soaking above and below the resonance field  $H^*$ .

frequency induction spectrometer with conventional lock-in detector and recorder. Because of the long relaxation times, it was necessary to use adiabatic fast-passage detection<sup>1</sup> similar to the techniques recently applied to quartz.<sup>2</sup> A typical plot of the dispersion derivative *vs* magnetic field is shown in Fig. 1, which illustrates the dependence of signal phase upon previous history. Before passing through resonance, the sample has been allowed to equilibrate with an external magnetic field under the conditions  $H_e > H^*$  and  $H_e < H^*$ , where  $H_e$  is the "soaking" field and  $H^*$  the resonance field. In one case the positive derivative occurs on the high-field side of the line and in the other case on the low-field side. The signal is symmetric because the adiabatic condition is fulfilled. However, as  $H_1$  is decreased so that  $\gamma H_1^2$  approaches  $\omega_m H_m$ , where  $H_0(t) = H_0 + H_m \cos \omega_m t$ , then the passage is no longer adiabatic with respect to the modulation field and the magnetization is destroyed by passing through the resonance.

The relaxation times measured by this technique are presented in Fig. 2 as a function of the mobile carrier concentrations. It can be seen that  $T_1$  is inversely proportional to the carrier concentration for the high-conductivity samples but approaches an asymptotic value in the purer samples. Bloembergen,<sup>3</sup> in his analysis of relaxation times in semiconductors, came to the conclusion that the relaxation of  $\text{Si}^{29}$  in the exhaustion and intrinsic ranges should be accomplished by an  $\mathbf{I} \cdot \mathbf{S}$  interaction between the nuclear spins and the spins of the mobile electrons or holes. His expression for relaxation by nondegenerate carriers, as modified by P. W. Anderson to include interband transitions and anisotropic masses, is

$$\frac{1}{2T_1} = \frac{256\pi\eta^2\beta^2\mu_I^2 N l}{9\hbar^4} \left( \frac{m_1 m_2 m_3 kT}{2\pi} \right)^{\frac{1}{2}},$$

where  $\eta = \psi^2(0)/\langle \psi^2 \rangle_{\text{Av}}$  over unit cell;  $N$  = density of mobile carriers;  $l$  = number of equivalent minima (six for *n*-type silicon), and  $m_1, m_2, m_3$  are the anisotropic

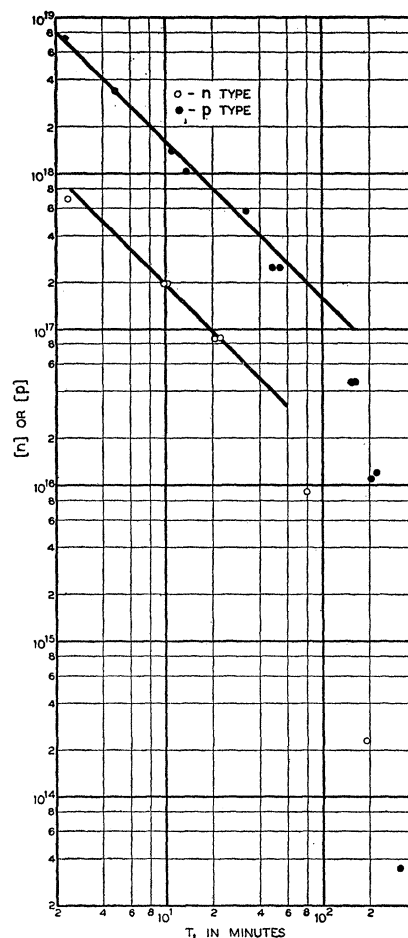


FIG. 2. Plot of  $\text{Si}^{29}$  spin-lattice relaxation times *versus* mobile carrier concentration.

effective masses. From this we calculate that for *n*-type silicon  $\eta = 186 \pm 18$ . The possible error arises from the uncertainty in the density of mobile carriers. The strength of the interaction in *p*-type silicon is smaller as can be seen from Fig. 1. This is expected because of the purely *p* nature of the hole wave functions. Several points of interest are:

(1) One of the *p*-type samples with  $1 \times 10^{16}$  mobile holes was an indium-doped sample. At 310°K there should be  $\sim 5 \times 10^{15}$  neutral indium acceptors. By a spin-diffusion mechanism,<sup>3</sup> considering the neutral indium atoms to be paramagnetic and perfect sinks, one can calculate that  $T_1$  should be several orders of magnitude smaller than the observed value. In some way the neutral acceptor's paramagnetism is not effective.

(2) The crystals were grown under different conditions, some pulled from quartz crucibles, some zone-refined without crucibles. No differences were observed because of this.

(3) The asymptotic values of *p*- and *n*-type silicon are different.

Measurements at lower temperatures and a more detailed discussion of these results and experimental techniques will be presented in the future.

We wish to thank Dr. P. W. Anderson for helpful discussions on the interpretation of these results and Dr. G. Feher for the loan of some equipment.

<sup>1</sup> F. Bloch, Phys. Rev. **70**, 460 (1946).

<sup>2</sup> Holzman, Anderson, and Koth, Phys. Rev. **98**, 542 (1955).

<sup>3</sup> N. Bloembergen, Physica **20**, 1130 (1954).

## dc Magnetoconductivity and Energy Band Structure in Semiconductors

R. M. BROUDY AND J. D. VENABLES

National Carbon Research Laboratories, National Carbon Company,  
A Division of Union Carbide and Carbon Corporation,  
Parma, Ohio

(Received June 26, 1956)

**T**HEORIES of the behavior of semiconductors under the influence of electric and magnetic fields give directly the magnetoconductivity tensor ( $L$ ), whereas the usual measurements give the magnetoresistivity tensor ( $P=L^{-1}$ ). The comparison of theory and experiment is ordinarily made by mathematical inversion of  $L$ . This procedure often proves unwieldy and limits the usefulness of the theory, usually restricting it to low or high  $H$  regions.

The purpose of this letter is to report an experimental method uniquely suited to the direct evaluation of the components of  $L$ . Application of this method to  $n$ -type germanium and silicon reproduces the known energy band structure.

Our technique consists in rotating  $H$  in one particular plane of crystalline symmetry, but in different sample planes in several experiments; all components of  $P$  can then be measured using only the usual Hall and resistivity probes—thence,  $L$  can be computed *vs* the position of  $H$  in the crystal plane. For cubic materials, which are here considered, only a single rectangular sample, cut with all three directions on axes of cubic symmetry, is required. The application to materials of other structure and to other directions in cubic materials becomes obvious.

Let  $\phi$  be the angle between  $H$  and a direction of cubic symmetry,  $H$  being rotated through a plane of cubic symmetry. Then Fig. 1 shows how one can obtain all four (the number is reduced due to the symmetry of the experiment) independent components of  $P(\phi)$  by measurement of  $P_{11}$  and  $P_{21}$  for both  $\phi$  and  $\psi$ . ( $P_{23}$  is the "planar hall" field first reported by Goldberg and Davis.<sup>1</sup>) We have thus far performed the experiment at 80°K for  $n$ -type germanium and silicon. The so-obtained  $L(\phi)$  contains considerable information about the band structure.

We have developed the theory for this experiment in the mass tensor approximation: Using the distri-

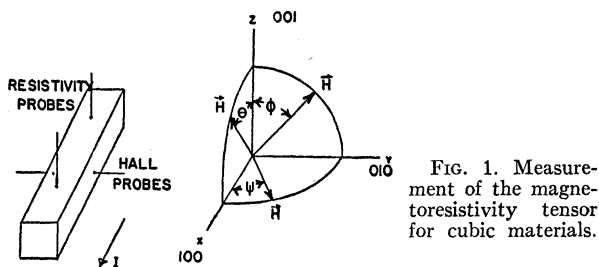


FIG. 1. Measurement of the magnetoresistivity tensor for cubic materials.

$$\begin{aligned} P_{11}(\phi) & P_{21}(\phi) & P_{31}(\phi) & = -P_{21}(90-\phi) \\ P_{33}(\phi) & = P_{11}(\psi) & P_{22}(\phi) & = P_{11}(90-\psi) & P_{23}(\phi) & = P_{21}(\psi) \\ P_{21}(\phi) & = P_{21}(\phi) & P_{22}(\phi) & = P_{11}(\phi) \end{aligned}$$

bution function of Blochinzev and Nordheim,<sup>2</sup> we obtain:

$$\mathbf{j} = -\frac{e^2}{4\pi^3} [\sigma^1 \mathbf{F} + (e/c) \rho^1 (M^{-1} \mathbf{F} \times \mathbf{H}) + (e/c)^2 \lambda^1 (M \mathbf{H} / |M|) (\mathbf{F} \cdot \mathbf{H})], \quad (1)$$

$$\sigma^1 \equiv \int \frac{(\partial f_0 / \partial E) \tau \mathbf{v} \mathbf{v} d\Omega}{1 + [e\tau/c]^2 (M \mathbf{H} \cdot \mathbf{H} / |M|)},$$

where  $\rho^1$  and  $\lambda^1$  are identical to  $\sigma^1$  but for the replacement of  $\tau$  by  $\tau^2$  and  $\tau^3$ , respectively. Using the relation  $\mathbf{v} = \hbar M^{-1} \mathbf{k}$ , a theorem of Herring<sup>3</sup> concerning the equality of energy shell averages, and the original distribution function of Bronstein,<sup>4</sup> Eq. (1) becomes

$$\mathbf{j} = -\frac{e^2}{6\pi^3} [\sigma M^{-1} \mathbf{F} + (e/c) (1/|M|) \rho (M \mathbf{H} \times \mathbf{F}) + (e/c)^2 (1/|M|) \lambda \mathbf{H} (\mathbf{H} \cdot \mathbf{F})], \quad (2)$$

$$\sigma = \int \frac{(\partial f_0 / \partial E) \tau(E) E d\Omega}{1 + [e\tau/c]^2 (M \mathbf{H} \cdot \mathbf{H} / |M|)},$$

with similar expressions for  $\rho$  and  $\lambda$  in  $\tau^2$  and  $\tau^3$ . Thus,

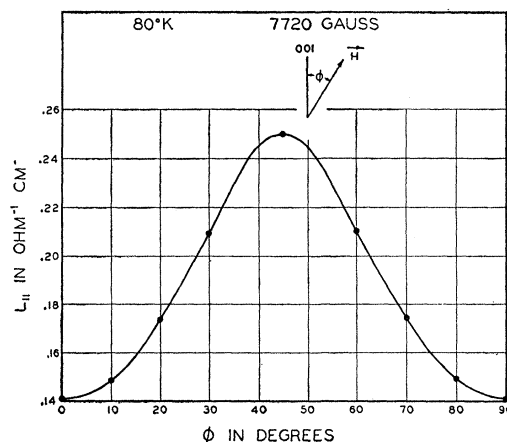


FIG. 2. Transverse magnetoconductivity for  $n$ -type germanium.